https://doi.org/10.5194/tc-2023-51
Preprint. Discussion started: 6 April 2023

The Cryosphere Discussions

Coupled thermo-geophysical inversion for permafrost monitoring

Soňa Tomaškovičová[1] and Thomas Ingeman-Nielsen[1]

[1]Department of Environmental & Resource Engineering, Technical University of Denmark, Nordvej 119, 2800 Kongens Lyngby, Denmark

Correspondence: Soňa Tomaškovičová (soto@dtu.dk)

Abstract. Conventional approaches in permafrost monitoring, including thermal measurements, core analyses and borehole geophysical logs, have drawbacks for long-term predictions of permafrost thermal state because of their discrete character and high cost. In order to accurately simulate and forecast thermal regime of the active layer and permafrost at a comparatively lower cost, we combined traditional thermal measurements with surface geophysical acquisitions. The fully coupled inversion scheme used only ground surface temperature data and time lapse geoelectrical measurements to calibrate a heat conduction model. The apparent resistivity data were incorporated into the coupled framework without being inverted separately, thus reducing the uncertainty inevitably associated with inverted resistivity models, especially on challenging permafrost terrain. The fully coupled modeling framework using field data achieved performance comparable to calibration on borehole temperature records, in terms of model fit within $0.6\,^{\circ}\mathrm{C}$, inversion convergence metrics as well as the predictive performance of the calibrated model.

1 Introduction

Numerical modeling is a powerful - and often the only available - tool for assessing the current and forecasting the future thermal state of permafrost (Riseborough et al., 2008; Harris et al., 2009). Models rely on quality data for forcing, calibration and validation. In thermal modeling of permafrost, calibration data are ideally ground temperature timeseries measured in boreholes, as these provide the most direct information about ground thermal regime. Boreholes are, however, geographically sparse while providing only discrete information in one spatial dimension. Meanwhile, the ground thermal regime is highly variable due to local conditions.

Surface geophysical measurements offer an attractive way of informing permafrost thermal models. Depending on the geophysical method used, they provide a 2D or 3D picture of subsurface properties, and cover comparatively large areas. Repeated measurements have been shown to hold information about in-situ processes, guiding development of more accurate process-based models. Studies by Hauck et al. (2008); Krautblatter et al. (2010); Tomaškovičová and Ingeman-Nielsen (in review) demonstrate that there is a quantitative link between electrical and thermal properties of geological materials.

In permafrost thermal modeling with field data, coupling approaches have been applied essentially in two ways: i) temperature-calibrated resistivity tomography has been used for quantitative estimation of ground ice and water content changes (Krautblatter et al., 2010), and ii) inverted resistivity models have been used to constrain ground ice changes estimates (Hauck et al., 2008). Tomaškovičová et al. (2012) presented a concept of the fully coupled thermo-geophysical inversion, where apparent

https://doi.org/10.5194/tc-2023-51
Preprint. Discussion started: 6 April 2023

electrical resistivity data before inversion are used to constrain optimization of heat model parameters. Jafarov et al. (2020) demonstrated the feasibility of the approach on synthetic datasets.

In this work, we evaluate performance of the fully coupled thermo-geophysical optimization framework on field monitoring data. We demonstrate that thermal parameters of a real ground undergoing phase change can be calibrated using time lapse geoelectrical measurements collected from the ground surface. Electrical properties of the ground depend mainly on the amount of unfrozen water available to carry the current. This unfrozen water content is temperature-dependent, and temperature at any depth depends on the surface energy balance (including water balance) and the soil thermal properties. We use electrical resistivity data for calibration because of their comparative ease of acquisition including possibility of automation, and relative ease and speed of data processing. However, any kind of geophysical data is in principle suitable, as long as the petro-physical relationship between ground temperature and the targeted geophysical property can be calibrated. Borehole temperature records are not needed for thermal model calibration in the fully coupled inversion approach; however where available, they may present valuable validation data. The workflow of the fully coupled thermo-geophysical inversion is explained in the following section.

2 The concept of the fully coupled thermo-geophysical inversion

The fully coupled thermo-geophysical inversion approach aims at predicting ground temperatures using geophysical measurements to calibrate thermal parameters of a ground thermal model. When using electrical resistivity data for calibration, the approach is built on the quantitative link between ground temperature and ground electrical properties (Hauck, 2002; Hauck et al., 2008; Doetsch et al., 2015; Oldenborger and LeBlanc, 2018). The ground electrical properties depend on four main factors: soil mineralogical composition, soil porosity, fraction of unfrozen water content and geochemical composition of the pore water (e.g. Hoekstra et al. 1975; Friedman 2005). The unfrozen water is typically the dominant conducting phase in a soil. It is also the only component that substantially changes its volume fraction over the course of a year, due to temperature-dependent processes of freezing and thawing (as well as due to drying and wetting in the unfrozen part of the year). Due to the zero-curtain effect, there is no single temperature value at which ground resistivity changes from frozen to unfrozen (Hauck, 2002; Doetsch et al., 2015; Tomaškovičová and Ingeman-Nielsen, in review). It is the unfrozen water content that quantitatively links the temporal changes in ground temperature with changes in ground electrical resistivity. The coupled inversion approach is outlined in Fig. 1 and further explained in the following paragraph.

The coupled model consists of two, essentially standalone, modules: a heat transport model (described in Sect. 4) and an electrical resistivity model (described in Sect. 5). The 1D heat transport model calculates a temperature distribution in the ground given a set of initial and boundary conditions and initial thermal parameters estimates. The calculated temperature distribution is then translated into a 1D multi-layer geoelectrical model by weighting the specific resistivities of the ground constituents by their temperature-dependent volumetric fractions. From the geoelectrical model, forward apparent resistivity response is calculated using the same electrode configurations as on the field site. The calculated apparent resistivities are compared to the field geoelectrical measurements. The difference is then minimized by adjusting thermal parameters of the

https://doi.org/10.5194/tc-2023-51
Preprint. Discussion started: 6 April 2023

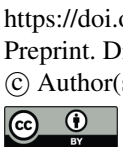

The Cryosphere
Discussions
Open Access
EGU

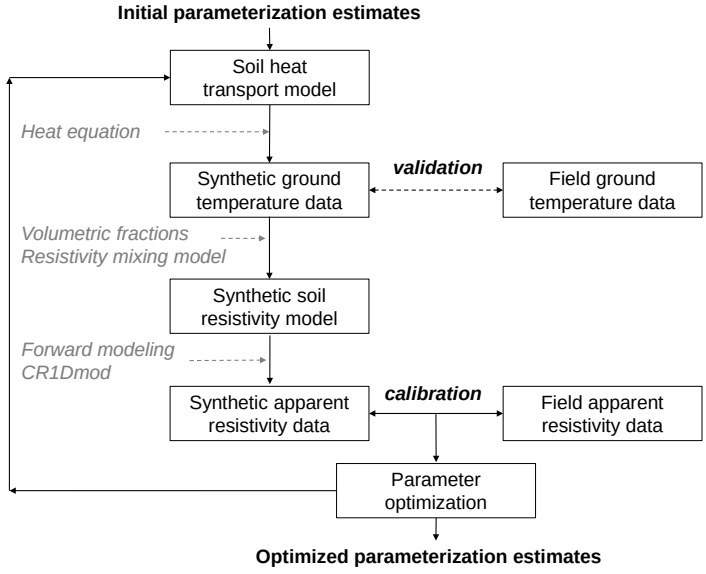

Figure 1. Flow diagram of the fully coupled thermo-geophysical inversion using ground surface temperature data as model forcing, and apparent resistivity data collected from the ground surface for calibration.

heat model from which the forward resistivities were calculated, and the specific resistivities of the soil constituents. The key characteristic of the fully coupled approach is the use of *apparent resistivities* for calibration, instead of inverted resistivity models. The reason for using apparent resistivities is the expectation that they introduce less additional uncertainty to the calibration in form of inherent inversion assumptions and artifacts. The relationship translating a certain ground electrical composition into apparent resistivity is unique, and governed by equations for conservation of charge, Ohm's law and the geometry of electrode configuration used to collect the resistivity data. Conversely, any inverted resistivity model is only one of a large number of possible realizations that explains the measured apparent resistivity data acceptably well. Interpretation of resistivity measurements from permafrost terrain in particular suffers from strong resistivity contrasts and ground ice features that may lead to over-estimating resistivity model parameters (Ingeman-Nielsen, 2005). The non-unique nature of the inverted resistivity models thus provides less solid basis for quantitative calibration.

The fully coupled modeling framework does not rely on borehole temperature data for the heat model calibration; ground surface temperatures, or possibly downscaled air temperatures, are needed to drive the heat transfer model. Naturally, when available, borehole temperature records are very useful resource for model validation and performance evaluation. We use borehole temperatures in our study to: i) validate the heat conduction model formulation and implementation (6.4), ii) validate the inverse problem formulation, and iii) to quantitatively assess the performance of the fully coupled inversion framework by comparing performance of the heat model calibrated on resistivities to the performance of the heat model calibrated on ground temperatures.

https://doi.org/10.5194/tc-2023-51
Preprint. Discussion started: 6 April 2023

3 Field site and data

The data used in this work come from an automated permafrost monitoring station in Ilulissat, West Greenland. The Ilulissat monitoring site (69° 14' N, 51° 3' W, 33 m above sea level) is situated ca. 200 m east of the airport in Ilulissat, on the mainland, in the inner part of the Disko Bay. The mean annual air temperature (MAAT) between 2010-2019 was $-3.1\,^{\circ}\mathrm{C}$ (data from Cappelen 2020). According to Obu et al. (2019) and Brown et al. (1998), the site is located in the continuous permafrost zone. Borehole temperature records from years 2012 – 2015 from the site (Tomaskovicova, 2018) advise the following permafrost parameters: the maximum active layer thickness is around 0.9 m, the ground temperatures at 4 m depth are in the range -3.0 to $-3.4\,^{\circ}\mathrm{C}$. The depth of zero annual amplitude is 5 m (defined as the depth of maximum annual amplitude < 0.1°).

The sedimentary profile in Ilulissat consists of fine-grained marine sediments deposited during the sea transgression following deglaciation of the area some 9600 BP (Bennike and Björck, 2002). The bedrock — Nagsugtoquidian gneisses with amphibolitic bands — is encountered at 7m depth according to borehole 78020 drilled as part of the site investigations for the nearby airport in 1978 (Geoteknisk Institut, 1978). The soil column is covered by a few cm thick vegetation layer.

Tomaškovičová and Ingeman-Nielsen (in review) have shown that the thermal regime in the sediments at the site is strongly influenced by hysteresis of unfrozen water content between freezing and thawing periods. The magnitude of this hysteresis justifies use of separate parameterization for the freezing and thawing periods, respectively.

4 Heat conduction model

We set up a ground thermal model based on the one-dimensional heat conduction equation with phase change (Lunardini, 1981):

$$\left(C_e + L\frac{\partial}{\partial T}\theta_w(T,x)\right)\frac{\partial}{\partial t}T(x,t) = \frac{\partial}{\partial x}\lambda_e\frac{\partial}{\partial x}T(x,t) \tag{1}$$

In this formulation T [°C] is temperature, L [J/m^3] is the volumetric latent heat of phase change between water and ice, θ_w is the volumetric unfrozen water content of the bulk soil [$\mathrm{m^3_{water}/m^3_{bulk}}$], C_e [J/m^3/K] and λ_e [W/m/K] are effective heat capacity and effective thermal conductivity, respectively, of the multi-phase media under consideration; x [m] is the depth below ground surface and t [s] is the time. Eq. 1 applies under the assumptions that there are no additional internal sources or sinks of heat, that no volume change is associated with the phase changes, that migration of water is negligible, and that there are no lateral variation in topography and soil properties (standard 1D assumption).

Dirichlet boundary conditions are applied at the top and bottom of the model (at depths $x = 0$ and $x = l$ respectively), such that $T(0,t) = T_u(t)$ and $T(l,t) = T_l(t)$, where subscripts u and l denote the upper and lower boundaries. A fixed temperature is used as bottom model boundary, as the yearly temperature amplitude at the bottom of 6 m deep borehole is < 0.09 °. The initial temperature distribution is specified throughout the model domain, such that $T(x,0) = T_0(x)$, where $T_0(x)$ is the temperature at depth x and time $t = 0\,\mathrm{s}$.

https://doi.org/10.5194/tc-2023-51
Preprint. Discussion started: 6 April 2023

Following Lovell Jr (1957) and Anderson and Tice (1972), we use a power function to describe the soil unfrozen water content variation at temperatures below freezing point:

$$\theta_w = \eta\phi, \quad \phi = \begin{cases} S & T \geq T^* \\ \alpha|T_f - T|^{-\beta} & T < T^* \end{cases} \tag{2}$$

where θ_w is the volumetric unfrozen water content of the bulk soil [$\mathrm{m^3_{water}/m^3_{bulk}}$], η is the porosity [$\mathrm{m^3_{voids}/m^3_{bulk}}$], ϕ is the volumetric unfrozen pore water fraction [$\mathrm{m^3_{water}/m^3_{voids}}$], S is the water saturation in completely unfrozen state [$\mathrm{m^3_{water}/m^3_{voids}}$] (assumed unity in this study) and α and β are empirical positive valued constants describing the intrinsic freezing characteristics of the given soil. T^* [°C] is the effective freezing point of the bulk soil – the lowest temperature at which all the water in the soil remains unfrozen ($\phi = S$) – and is given by:

$$T^* = T_f - \left(\frac{S}{\alpha}\right)^{-\frac{1}{\beta}} \tag{3}$$

where T_f [°C] is the freezing point of the pore water as a free substance.

Given a certain value of unfrozen water content, and under the assumption that the soil is fully saturated at all times, the volumetric fractions of soil particles θ_s and ice θ_i (constants) are derived as:

$$\theta_s = 1 - \eta, \quad \theta_i = \begin{cases} 0 & T \geq T^* \\ \eta(S - \phi) & T < T^* \end{cases} \tag{4}$$

Pronounced hysteresis in the unfrozen water content variation (e.g. Pellet and Hauck (2017); Pellet et al. (2016); Overduin et al. (2006)) and its effect on the yearly enthalpy change normally requires that two separate parameterizations – (α_f, β_f) for the freezing season and (α_t, β_t) for the thawing season in Eq. (2) – are used, to accurately model the freezing and thawing processes respectively. In this modeling exercise, we use data from the freezing seasons only, therefore our notation (α, β) relates to the freezing curve parameterization (instead of notation (α_f, β_f)).

The effective parameters of a bulk, three-phase soil are derived as a function of their respective volumetric fractions, which are essentially a function of temperature. The effective heat capacity C_e is expressed as the sum of the specific heat capacities of the soil phases weighted by their volumetric fractions (e.g., Anderson et al., 1973):

$$C_e = C_s\theta_s + C_w\theta_w + C_i\theta_i \tag{5}$$

Common Johansen's thermal parameterization (geometric mean) is used for modeling the effective thermal conductivity λ_e of a n-phase soil (Johansen, 1977; Zhang et al., 2008):

https://doi.org/10.5194/tc-2023-51
Preprint. Discussion started: 6 April 2023

$$\lambda_e = \prod_{j=1}^{N} {\lambda_j}^{\theta_j} \tag{6}$$

To solve the heat conduction equation, we used an in-house code SOILFREEZE1D which implements a finite-difference scheme on a fixed grid with equidistant nodes. The code uses the unconditionally stable Crank-Nicholson algorithm with adaptive time-stepping to minimize errors in the solution. For sufficiently small time-steps, the analytical derivative of Eq. (2) may be used to estimate the change in unfrozen water content. However, to allow manageable step-sizes, we implemented an iterative scheme for the change in water content. The first iteration for each time-step uses the analytical derivative, while subsequent iterations use a finite difference, based on the temperature estimate resulting from the previous iteration. Iterations proceed until the maximum change in estimated temperature is less than a specified threshold, or until a specified number of iterations have completed, in which case the time-step is reduced.

The lithology at the Ilulissat field site – waterloggeds silty clays with low hydraulic conductivity – justifies that a number of simplifying assumptions are made in the interest of maintaining the model parsimony:

1. Heat conduction is assumed to be the dominant mechanism of heat transport, considering that conditions for water movement are limited to summer (Jessen et al., 2014), thus essentially outside of the time period used for calibration (September-February);

2. The ground is assumed to be fully-saturated (an assumption previously used eg. by Nicolsky et al. (2007) and Romanovsky et al. (2000)), thus consisting of up to three constituents: soil particles, water and ice;

3. The ground is assumed to be homogeneous, thus neglecting any lithological layers or varying thermal properties. While we mention in Sect. 3 that up to four layers can be identified in the soil depending on thermal state of the ground, results of our experiments with heterogeneous model setup (not reported here) did not substantially improve model performance to justify the increased complexity.

4. Specific heat capacity and specific thermal conductivity of the respective soil constituents are assumed constant. This is an acceptable approximation considering that using constant parameters results in errors of less than 10% in the temperature range between $-20\,^{\circ}\mathrm{C}$ to $0\,^{\circ}\mathrm{C}$ (Osterkamp, 1987);

5. Latent heat of phase change is assumed constant;

6. A fixed temperature is used as bottom model boundary. This is an acceptable simplification when modeling relatively short temperature timeseries, and considering that measured yearly temperature amplitude at the bottom of $6\,\mathrm{m}$ deep borehole is $< 0.09\,^{\circ}$.

Choice of model discretization in time and space was based on convergence testing. For this modeling experiment, the heat model domain was set to be $6\,\mathrm{m}$ deep. The comparatively shallow model was adequate considering the relatively short

https://doi.org/10.5194/tc-2023-51
Preprint. Discussion started: 6 April 2023

timeseries we modeled – up to 180 days, given by the need for separate parameterizations of freezing and thawing seasons (Sect. 3). We specified equidistant mesh for the heat model solution with nodes every $0.05\,\mathrm{m}$, and we limited the maximum step size of the differential equation solver to $1\,\mathrm{h}$. The forcing data for the model were ground surface temperatures collected every 3 hours. The fixed temperature at the model bottom boundary was informed by the observations from the $6\,\mathrm{m}$ deep borehole, located ca. $10\,\mathrm{m}$ away from the resistivity acquisition line.

The modeling and inversion frameworks were implemented in MATLAB, with the heat equation solver implemented in PYTHON using the *numpy* module for optimized array and matrix computations.

5 Resistivity model

The geophysical part of the modeling framework consists of a 1D forward geoelectrical model. Through convergence testing, we determined that 128 layers of equal thickness produced convergent solution for the $6\,\mathrm{m}$ deep model. A representative temperature was assigned to each resistivity model layer by interpolating the nearest heat model solution. Fractions of water, ice and soil minerals in each layer were calculated based on Eq. (2) and Eq. (4). The effective bulk resistivity ρ_e of each resistivity model layer was then derived using a resistivity mixing relationship. We tested two commonly used resistivity mixing relationships: i) the Archie's law, and ii) the geometric mean model, to identify the one with resistivity parameters more sensitive to calibration in the fully coupled inversion scheme (Fig. 7).

The traditional Archie's law (Archie et al., 1942) derives effective bulk resistivity of ground material based on material's porosity and on a resistivity of the pore fluid:

$$\rho_e = \rho_w \eta^{-m} \phi^{-n} \tag{7}$$

where ρ_e is the effective resistivity of the bulk soil, ρ_w is the specific resistivity of the pore water, η is the porosity, ϕ is the unfrozen fraction of pore water and m and n are empirical coefficients.

The geometric mean model (eg. Guéguen and Palciauskas (1994)) estimates the effective bulk resistivity as the geometric mean of specific resistivities of the respective ground components, weighted by their volumetric fractions:

$$\rho_e = \left(\prod_{i=1}^{n} \rho_i^{\theta_i} \right) \tag{8}$$

where ρ_i and θ_i are the specific resistivity and volumetric content of the i-*th* soil constituent respectively.

Based on the derived effective ground resistivity model, synthetic apparent resistivities ρ_s were forward-calculated using CR1DMOD code (Ingeman-Nielsen and Baumgartner, 2006), using the same electrode configuration as in the field acquisitions. As the apparent resistivity field measurements were launching every day at 18:00 UTC and last for up to 5.5 hours, heat model solutions at time steps between 18:00 – 00:00 UTC every day were averaged to provide the temperature profile corresponding to the timing of the resistivity acquisitions.

https://doi.org/10.5194/tc-2023-51
Preprint. Discussion started: 6 April 2023


The Cryosphere Discussions
Open Access
EGU

6 Validation of the heat model and of the inverse problem formulation

Prior to utilizing the heat model as part of the coupled inversion, we evaluate its ability to reproduce real ground temperature dynamics. We also evaluate performance of the optimization algorithm and identify a strategy for effective multi-parameter optimization.

6.1 Choice of the target parameters for optimization

Approaching an inverse problem begins with identifying a subset of model parameters to be targeted by the optimization, as optimization with respect to all model parameters is not feasible. Diagnostic statistics can measure the amount of information for parameter calibration in the available data, and can inform the choice of parameters that can be effectively recovered from the data (Hill, 1998).

Scaled sensitivities (SS) (Hill, 1998) compare the importance of different observations to the estimation of a single parameter (or, the importance of different parameters to the calculation of a simulated value). SS can help to identify the time periods in calibration data with most information for calibration of the target parameter. SS are calculated as:

$$ss_{ij} = \left(\frac{\delta y'_i}{\delta v_j}\right) v_j \sqrt{\omega}_i \tag{9}$$

where y'_i is a simulated value, v_j is the j$^{\text{th}}$ estimated parameter, $\left(\frac{\delta y'_i}{\delta v_j}\right)$ is the sensitivity of the simulated value to the j^{th} parameter, and is evaluated at V, V is the vector which contains the parameter values at which sensitivities are evaluated, and ω_i is the weight of the i^{th} observation.

To evaluate relative importance of respective model parameters for the model predictions, we calculate the composite scaled sensitivities (CSS) (Hill, 1998) for each of the parameters of the heat model. Fig. 2 shows the change in simulated temperature field caused by 10 % increase in each of the evaluated parameters. Because the calibration problem is nonlinear with respect to many parameters of interest, the sensitivity of the evaluated parameter will change for different values of parameters in the parameters vector V, as well as for different model discretizations in time and space. An exhaustive sensitivity analysis at every inversion iteration would, however, be computationally inefficient. Assuming some degree of linearity in the model response to each parameter input, carefully chosen starting point will be descriptive for sensitivity of each of the fitted parameters. Less influential parameters, as well as parameters with well-known table values were fixed during the actual optimization. The most sensitive parameters were then calibrated in a multi-parameter optimization. Refer to the Table 1 for overview of the fixed and fitted parameters.

According to Fig. 2, before calibration, parameters C_w (heat capacity of water), C_i (heat capacity of ice), k_w (thermal conductivity of water), k_i (ice) and T_f had relatively less influence on the heat model calculations and thus are fixed to table values or an empirical small value (T_f). Parameters C_s and k_s (heat capacity and thermal conductivity of mineral grains), α and β (freezing/thawing parameters), and porosity (η) are soil-specific properties with substantial influence on model predictions.

https://doi.org/10.5194/tc-2023-51
Preprint. Discussion started: 6 April 2023

The Cryosphere
Discussions
Open Access
EGU

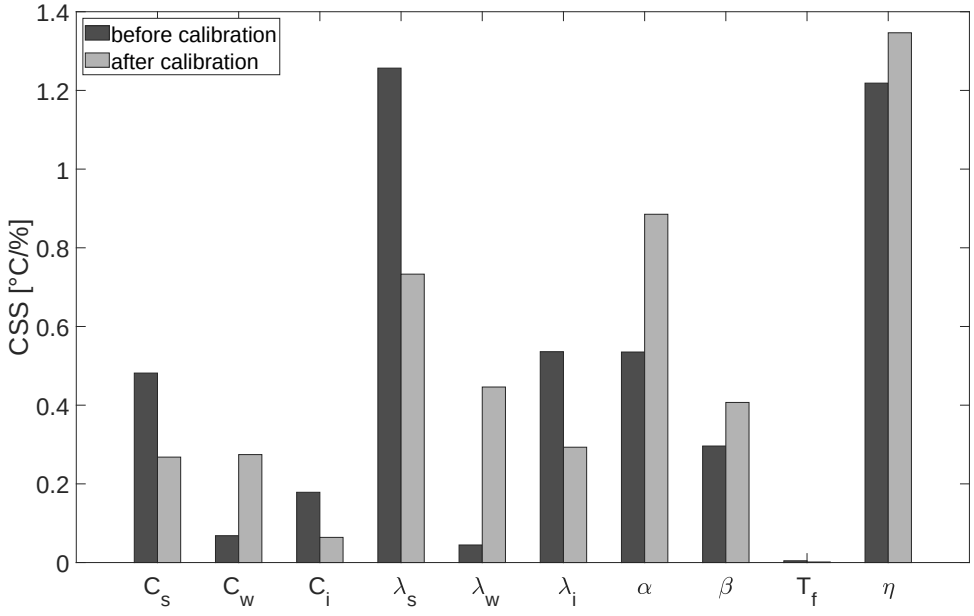

Figure 2. Composite scaled sensitivities (CSS) of 10 parameters of the 3-phase heat conduction model, before and after calibration. CSS corresponds to the change in simulated temperature field caused by 10% increase in the evaluated parameter. Parameters: C_s, C_w, C_i – heat capacities of soil grains, water and ice, resp.; k_s, k_w, k_i – thermal conductivities of soil grains, water and ice, resp.; α, β – soil freezing parameters; T_f – freezing point of water as a free substance; η – porosity.

After calibration, porosity remained the key parameter for model predictions. Importance of α and β parameters slightly increased, while influence of heat capacity and thermal conductivity of mineral phase has relatively decreased.

Table 1. Parameterization of the heat model. For the *fixed parameters*, we show their fixed values in the optimization. For the *fitted parameters*, we list their bounds – maximum and minimum values that the optimization algorithm is permitted to investigate when searching for the optimal parameter value.

Fixed parameters	Value	Fitted parameters	Bounds
C_w	4.19e6 J/m^3/K	C_s	0.6e6 – 4.1e6 J/m^3/K
C_i	1.9228e6 J/m^3/K	λ_s	0.5 – 8 W/m/K
λ_w	0.56 W/m/K	η	0.1 – 0.9
λ_i	2.18 W/m/K	α	0.1 – 5
T_f	$-0.0001\,^\circ$C	β	0.01 – 5

220 Fig. 3 shows the scaled sensitivity for each of the five fitted parameters of the heat model. As expected, the periods of time when the ground undergoes phase change contained the most information for estimation of each given parameter. Ground temperature cooling from around $-2\,^\circ$C and lower appears to be the most important part of data acquisition for the model

https://doi.org/10.5194/tc-2023-51
Preprint. Discussion started: 6 April 2023

The Cryosphere Discussions
Open Access
EGU

calibration. This could be eg. due to ice formation that have progressed enough to alter the bulk thermal properties of the ground as suggested by the highest sensitivity of porosity η to this part of the dataset.

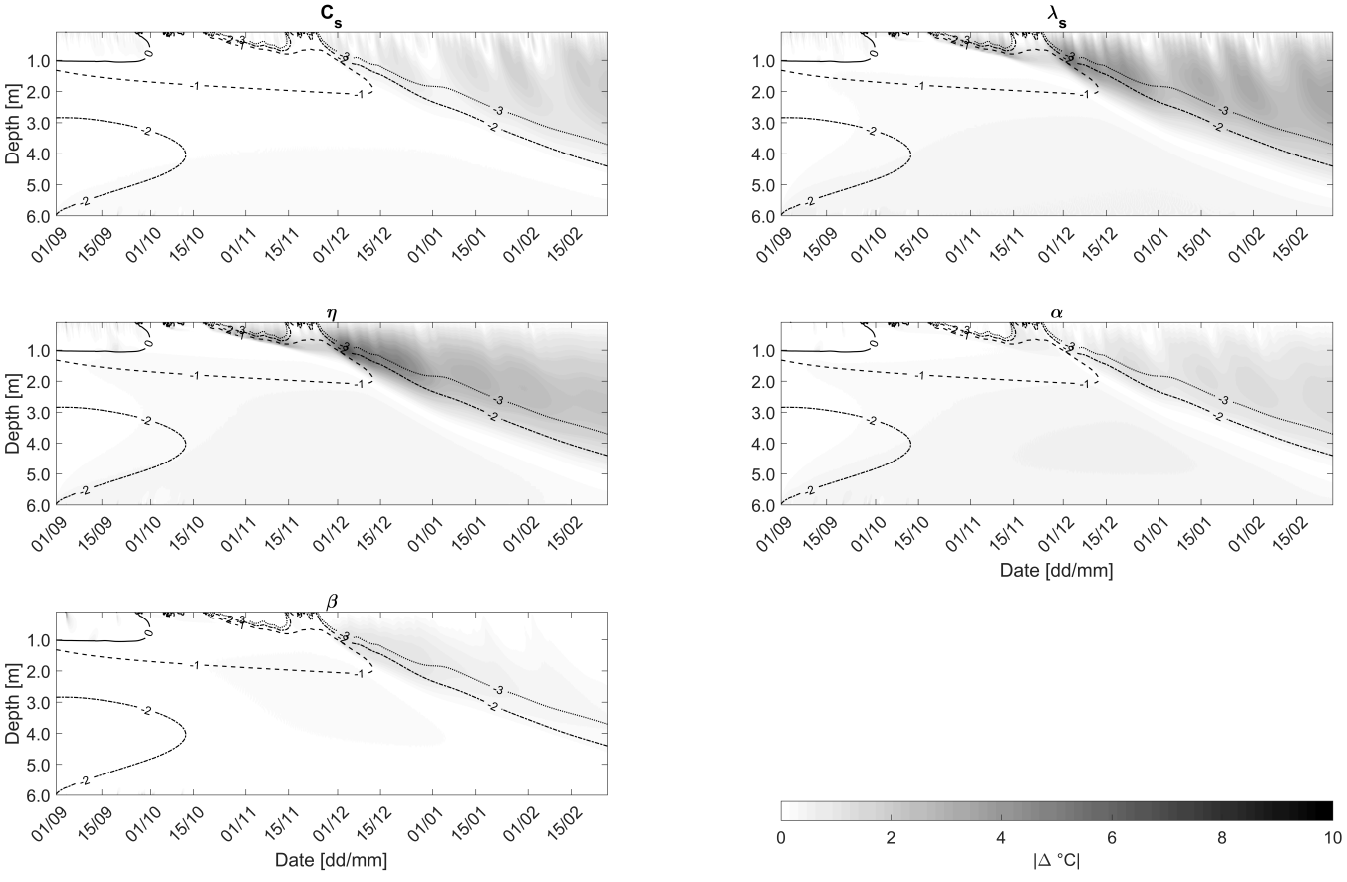

Figure 3. Scaled sensitivities of the 5 fitted parameters of the 3-phase heat conduction model. Intensity of the grey shading corresponds to the absolute value of change in the simulated temperature value caused by 10% increase in the evaluated parameter. Contour lines with various dashing correspond to isotherms of the ground freeze-up period.

6.2 Inverse problem formulation

To describe the inverse problem we adopt the notation from (Nicolsky et al., 2007) and (Nicolsky et al., 2009). We define the vector V as consisting of the fitted thermal parameters: $V = \{C_s, \lambda_s, \alpha, \beta, \eta\}$. For each physically realistic control vector V, it is possible to compute temperature dynamics and compare it to measured borehole data. The measured data are organized in a vector d in form of averages of eight daily temperature records at each sensor depth. The data d are related to the control vector V by $m(V) - d = e$, where m is the modeled counterparts of the data and e is the misfit vector. In theory, if there are no

https://doi.org/10.5194/tc-2023-51
Preprint. Discussion started: 6 April 2023

measurement errors or model inadequacies, the misfit vector e can be reduced to zero. If there are errors in the data or in the model, the aim is to minimize e by varying the control vector V.

The heat model optimization uses trust-region reflective algorithm based on the interior-reflective Newton method (Coleman and Li, 1996), as implemented in the MATLAB solver *lsqnonlin*. The cost function is the root mean square error (RMSE) between measured and simulated ground temperatures. Convergence is identified by meeting at least one of the two criteria: either 1) the change of parameter value, or 2) the change in the RMSE between previous and current iterations should be smaller than a prescribed tolerance.

Specifying *bounds* for the fitted parameters spares the solver from examining physically implausible parameter values. An overview of the fixed and fitted parameters, along with their upper and lower bounds is provided in Table 1.

To identify a viable combination of fitted parameters that can be calibrated simultaneously, we first test the calibration approach in two synthetic scenarios, with and without noise (Sect. 6.3), before applying it to the field data (Sect. 6.4).

6.3 Heat model validation on synthetic data

Heat model parameters in the control vector V were set to arbitrary – though realistic – values. These values were considered the *true parameter values* (V_t) and were used to calculate a temperature field $m(V_t)$ in the forward problem (Eq. 1); we termed this temperature field the *reference temperature field*. Next, the control vector V_t was perturbed with an error coefficient $e = [0.5, 1]$ so that the $V_p = V_t \pm e \times V_t$. The resulting temperature field calculated was called the *perturbed temperature field*. We then minimized the RMSE between the perturbed and the reference temperature field by optimizing for one to five of the perturbed fitted parameters at once. The heat model solutions at mesh nodes every $0.1\,\mathrm{m}$ between $0.1\,\mathrm{m}$ to $1.5\,\mathrm{m}$ depth were used in the objective function. This corresponds to the real-life situation, where temperature measurements are typically available from only a limited portion of the soil profile. To force both the reference and perturbed temperature field calculations, we used ground surface temperatures available from the MRC sensor at this site (Tomaškovičová and Ingeman-Nielsen, in review). Bottom boundary at $6\,\mathrm{m}$ was set to $-3.1°$ based on borehole information from the area.

Each one of the fitted parameter of the heat model ($C_s, \lambda_s, \alpha, \beta, \eta$) converged towards its *true value* in the single-parameter optimization on synthetic data without noise. For porosity (η), the most sensitive parameter of the model, starting the single-parameter calibration from anywhere within the parameter bounds (0.1 - 0.9), the optimization converged to the true value (0.3) within 7 iterations, with RMSE in the order of 10^{-4}. β was the least sensitive of the fitted parameters; nevertheless, the optimization converged to its true value within 4 iterations, with RMSE in the order of 10^{-4} to 10^{-3} depending on the initial guess. All the parameters were well-determined with narrow 95%-confidence intervals.

We simulated a case of having *half the amount of calibration data* by using the heat model solutions at mesh nodes every $0.2\,\mathrm{m}$ between $0.1\,\mathrm{m}$ to $1.5\,\mathrm{m}$ depth (instead of every $0.1\,\mathrm{m}$. The reduced amount of calibration data did not influence convergence performance of the model – neither the number of iterations nor the RMSE after inversion increased.

In practical applications, *daily averages* may be used for model forcing and calibration. When using daily averages for forcing the calculation of the perturbed temperature field and for the objective function, the optimization algorithm needed one

https://doi.org/10.5194/tc-2023-51
Preprint. Discussion started: 6 April 2023

more iteration to converge. Nevertheless, accuracy of the solution was not affected and true parameter values were accurately recovered.

Up to four parameters could be estimated at once. The joint optimization for the four parameters λ_s, α, β and η converged within 26 iterations. The recovered parameters were found within 15 % from their true values.

In the next experiment, we added random *noise* with amplitude $\pm 0.03\,^{\circ}\mathrm{C}$ to each of the 'measurements' of the reference temperature field. The perturbed parameters were then recovered by optimizing on this 'noisy' reference temperature field. True values of all the fitted parameters were recovered in single-parameter calibration starting from an initial guess up to 50% higher than the true parameter value. Equally, performance of the four-parameter calibration with noise was comparable to the case without noise – recovered parameters laid within 15% from their true values.

Attempting joint calibration of all five fitted heat model parameters C_s, λ_s, α, β and η caused the optimization to converge towards a solution relatively far from the true parameter values. This approach was therefore deemed not viable. A way to get around fitting the fifth parameter C_s was to define an plausible range for the C_s values, then run a sequence of 4-parameter optimizations with C_s fixed at every step of the predefined range. In result, we obtained a RMSE value for four-parameter optimizations with C_s fixed at respective values of the predefined range (such as in Fig. 4a that shows such results for the field, instead of the synthetic, dataset). We call this the *4+1 optimization approach* and we use it in the next validation step: validation of the heat model on field borehole temperature measurements (section 6.4).

The calibration tests on synthetic datasets confirmed that the trust-region reflective algorithm can recover true parameter values even in scenarios with reduced amount of calibration data, with noisy calibration data, and is not affected by the use of daily averages instead of individual temperature records. We thus deem the inversion algorithm well-suited for handling our optimization problem, provided that right optimization settings are used. The essential settings for optimal performance of the optimization are the convergence tolerances, size of finite-difference steps, and upper and lower bounds on the permitted parameter value range.

6.4 Heat model validation on field data

The next step following the synthetic tests was to confirm that our heat model succeeds at recovering thermal parameters of a real ground. This meant to optimize the thermal parameters on borehole temperature timeseries instead of synthetic reference temperature field.

Initial and boundary conditions were identical as in the synthetic tests (Sect. 6.3) as these came from a sensor at the site. The difference was that the reference temperature field in this case were the actual in-situ ground temperature timeseries measured by the MRC probe in the depth between $0.1\,\mathrm{m}$ to $1.5\,\mathrm{m}$ during freezing season 1$^{\mathrm{st}}$ September 2014 – 28$^{\mathrm{th}}$ February 2015 (for description of the sensors and datasets, refer to Tomaskovicova (2018)). The reason to choose the shallow MRC probe records was that they provided the longest uninterrupted series of boundary conditions for forcing our model.

We used the *4+1 optimization approach* developed in the synthetic tests (Sect. 6.3). As a maximum of four parameters could be calibrated at once, we began by defining a plausible range for the fifth parameter C_s as 0.6e^6 – 4.1e^6 J/m^3/K, subsequently narrowed down to 2.4e^6 – 3.7e^6 J/m^3/K. We then ran a total of 92 4-parameter optimizations of the remaining fitted parameters

https://doi.org/10.5194/tc-2023-51
Preprint. Discussion started: 6 April 2023

α, β, η, and λ_s, with C_s fixed at 0.1e^6-increments of the pre-defined range. The summary of all the optimization runs is provided in Table 2, including the 'Initial' and the 'Optimized' parameter values, average error after optimization ('Minimum RMSE') and the confidence intervals.

Table 2. Summary of the 92 calibration runs on field data using the *4+1 optimization approach*. The 'RMSE1' shows the 'Minimum RMSE' from 36 optimizations runs, each starting with C_s fixed at 0.1e^6-increments between 0.6e^6 – 4.1e^6 J/m^3/K and remaining parameters $[\alpha, \beta, \eta, \lambda_s]$ starting from the 'Initial' values. The 'RMSE2' through 'RMSE5' show 'Minimum RMSE' from 14 calibration runs each, starting with C_s fixed at 0.1e^6-increments between 2.4e^6 – 3.7e^6 J/m^3/K (narrower C_s range) and the remaining four fitted parameters starting from the 'Initial' values as specified. The 95% confidence intervals ('95% CI') indicate the range of values that one can be 95% certain contains the true mean value of the parameter.

Run	Parameter	Initial	Optimized	95% CI	Minimum RMSE
RMSE1	C_s	0.6e^6 – 4.1e^6	3e^6	–	0.5517
	α	0.21	0.7468	± 0.0064	
	β	0.60	0.1006	± 0.0089	
	η	0.30	0.5258	± 0.0198	
	λ_s	2.00	1.7136	± 0.0955	
RMSE2	C_s	2.4e^6 – 3.7e^6	2.9e^6	–	0.5515
	α	0.10	0.7738	± 0.0053	
	β	0.20	0.0839	± 0.0070	
	η	0.40	0.5935	± 0.0172	
	λ_s	3.00	2.0573	± 0.1328	
RMSE3	C_s	2.4e^6 – 3.7e^6	2.4e^6	–	0.5509
	α	0.40	0.7916	± 0.0040	
	β	0.55	0.0792	± 0.0059	
	η	0.35	0.6308	± 0.0145	
	λ_s	1.80	2.2407	± 0.1413	
RMSE4	C_s	2.4e^6 – 3.7e^6	2.5e^6	–	0.5523
	α	0.32	0.8129	± 0.0033	
	β	0.70	0.0719	± 0.0049	
	η	0.60	0.7276	± 0.0113	
	λ_s	2.20	4.1891	± 0.3923	
RMSE5	C_s	2.4e^6 – 3.7e^6	2.7e^6	–	0.5503
	α	0.50	0.7482	± 0.0061	
	β	0.58	0.1045	± 0.0090	
	η	0.20	0.5012	± 0.0188	
	λ_s	1.90	1.5080	± 0.0713	

https://doi.org/10.5194/tc-2023-51
Preprint. Discussion started: 6 April 2023

The Cryosphere Discussions
Open Access
EGU

The smallest average error ('RMSE5' = 0.5503) between the field and simulated temperature fields was found for the following parameter combination: C_s = 2e7 J/m^3/K, α = 0.75, β = 0.10, η = 0.50 and λ_s = 1.51 W/m/K (Table 2). This optimization run took 14 iterations to converge. The fit between the field measurements and the temperature field calculated with these parameter values is shown on Fig. 4b. It shows consistently good agreement of the simulations with observations, particularly in the portion of the dataset below the freezing point. The highest misfit is associated with temperatures above freezing point – when the ground temperature is not largely controlled by phase change processes and water movement and evaporation of the soil moisture may potentially influence the bulk thermal properties.

It is however important to point out that the changes in RMSE between all the 92 optimization runs were very small – below precision of our temperature sensor – in spite of the large range of C_s values evaluated (Fig. 4a). This suggests two conclusions; first, that our implementation of the heat model is not sensitive enough to the parameter C_s to enable its calibration. Second, the final model is starting model-dependent, which is reflected in the spread of the optimized parameter values producing practically the same model fit. We can therefore expect that the optimized parameter values are not the true ground thermal properties, however they reflect them well enough to simulate the temperature field within $0.6\,^{\circ}$C of the field measurements, on average.

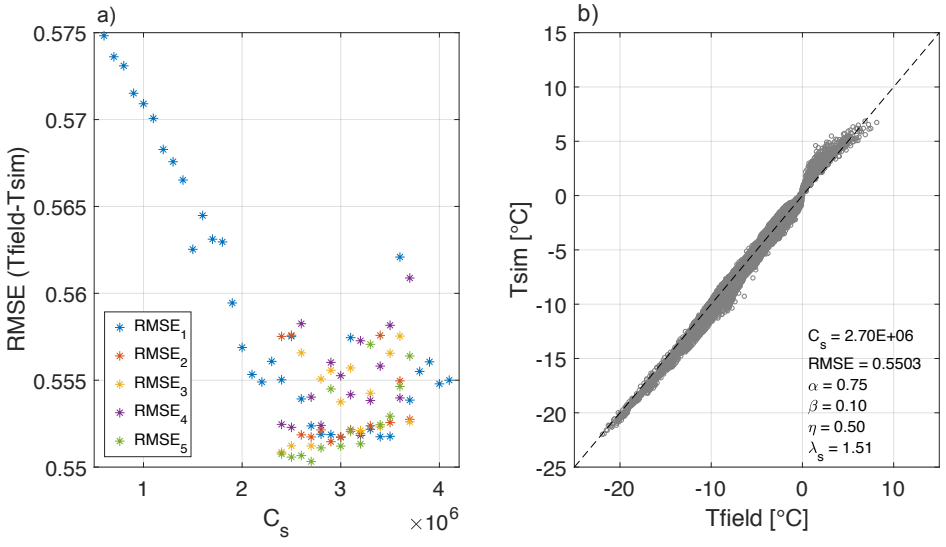

Figure 4. (a) RMSE after optimization for the 92 model runs starting from different initial parameter estimates. The same-color markers indicate the calibrations starting from the same initial values for parameters α, β, η and λ_s (as specified in Table 2), and the initial value for C_s fixed on 0.1e6-increments in the specified range (0.6e^6 – 4.1e^6 J/m^3/K for the group of runs RMSE1, and 2.4e^6 – 3.7e^6 J/m^3/K for RMSE2 – RMSE5). (b) Crossplot of field-measured temperature field vs. the temperature field simulated with parameters optimized in the 'RMSE5' run; the optimized parameter estimates are indicated in the annotation. The average misfit between simulated and field temperatures is $0.55\,^{\circ}$C.

https://doi.org/10.5194/tc-2023-51
Preprint. Discussion started: 6 April 2023

315 Figure 5 shows the analysis of differences between the field-measured vs. simulated (using 'RMSE5' parameterization) temperatures at five depths throughout the active layer (0 to 0.9 m) and top of permafrost (below 0.9 m). Predictably, the model struggles to accurately reproduce amplitudes of rapid temperature fluctuations in the shallow subsurface and introduces smoothing and lag into the simulated temperature timeseries. Overall, above the freezing point, the model introduces a warm bias, with simulated temperatures warmer than field measurements; conversely, below the freezing point, the model exhibits
320 a cold bias. These observations suggest that the thermal conductivity λ_s in the model may be over-estimated compared to the properties of the real ground. Permafrost temperatures (below 0.9 m) are reproduced more accurately, possibly because the ground spends more time in the phase transition around 0°, which the model reproduces very well. This suggests that the soil freezing curve parameters (α, β) are close to the real soil values.

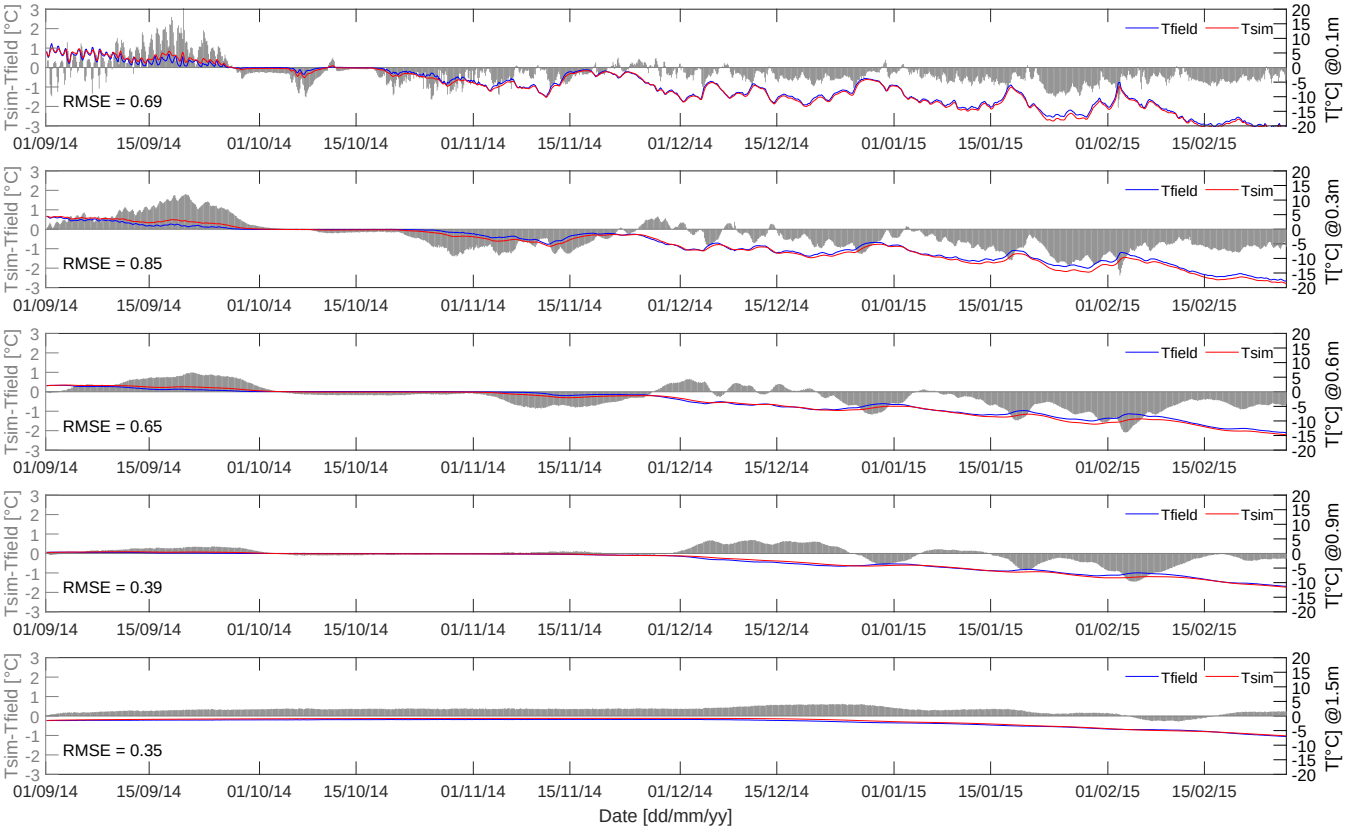

Figure 5. Performance of the heat model calibrated on borehole temperatures evaluated shown as differences between simulated vs. measured ground temperature timeseries at five different depths across the active layer and top of permafrost (below 0.9m) during the freezing season 2014/2015.

Since sensitivity of a model to input parameters changes with changing values of these parameters, we repeated the sensitivity
325 analysis from Sect. 6.1 using the calibrated parameter values ('RMSE5'). The CSS analysis confirmed the importance of the fitted parameters C_s, α, β, η and λ_s for heat model predictions and did not reveal new optimization targets (Fig. 2, after

https://doi.org/10.5194/tc-2023-51
Preprint. Discussion started: 6 April 2023

calibration). We accepted the model calibrated in the 'RMSE5' optimization run as well performing model with physically plausible parameter values, and we proceeded to validate these in the following Sect. 6.5.

6.5 Validation of the optimized heat model parameter values

Direct measurements of the heat model parameters were not available, except for porosity η, which was found to be between 0.40 – 0.62 depending on the exact location near the site, and depth (Pedersen, 2013). Thus we chose to validate the model calibration by data-splitting (Power, 1993). This was done by using the parameter values optimized on the freezing season 2014/2015 to predict temperature regimes in the previous freezing seasons 2012/2013 and 2013/2014, respectively.

The model calibrated on freezing season 2014/2015 ('RMSE5' parameterization) predicted ground temperatures measured between 1st November 2012 – 28th February 2013 within $\pm$ 0.63°(Fig. 6a). The measurements from freezing season 2013/2014 (only two months between 1st September 2013 — 29th October 2013 available) were reproduced within $\pm$ 0.32°(Fig. 6b).

We consider the results of the 'RMSE5' optimization run our best approximation of the actual ground thermal properties in Ilulissat, and we refer to these values when evaluating the performance of other inversion approaches.

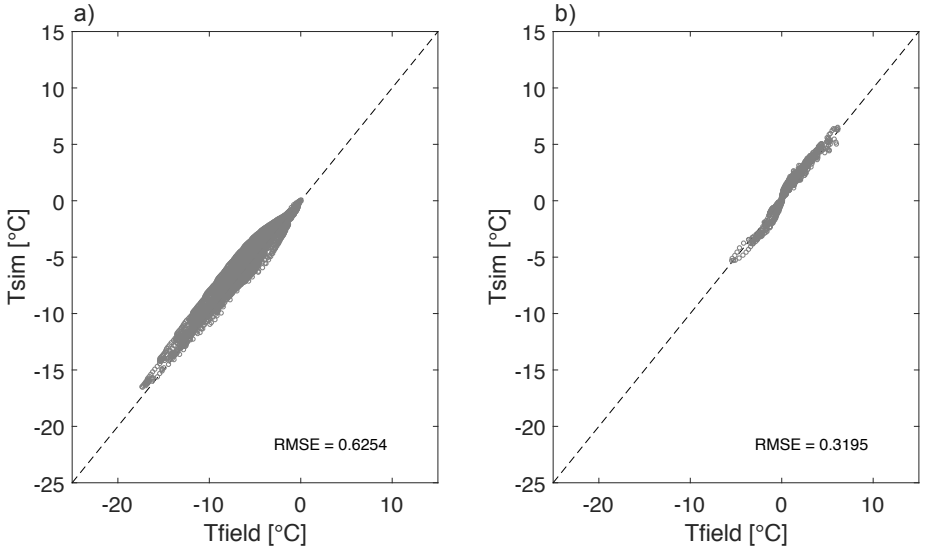

Figure 6. (a) Validation of the heat model calibration on freezing season 2012/2013, data between 1st November 2012 – 28th February 2013. (b) Validation on freezing season 2013/2014. data between 1st September 2013 – 29th October 2013.

7 The fully coupled thermo-geophysical inversion

We describe the choice of petro-physical relationship for the resistivity model, then validate the coupled optimization approach on synthetic data before evaluating performance of the fully coupled inversion scheme in comparison to calibration on borehole temperatures.

https://doi.org/10.5194/tc-2023-51
Preprint. Discussion started: 6 April 2023

7.1 Choice of the resistivity model parameterization

Sensitivity analysis was repeated for the fully coupled optimization scheme to identify the more suitable petro-physical formulation for use in the resistivity model (Sect. 5). Both thermal and resistivity parameters were evaluated, as success of the coupled optimization depends on sensitivity of the forward apparent resistivity calculation to change in the heat parameters (C, λ), as well as the resistivity parameters (ρ of the water, ice and soil minerals, Archie's parameters m and n). Parameters α, β, T_f, and η describe the unfrozen water content variation with temperatures below freezing point and are common to both heat and resistivity modules in the coupled scheme. Figure 7 shows changes in simulated apparent resistivity (log-transformed) resulting from 10% change in each of the input parameters for the two petro-physical relationships evaluated – the geometric mean model and the Archie's law.

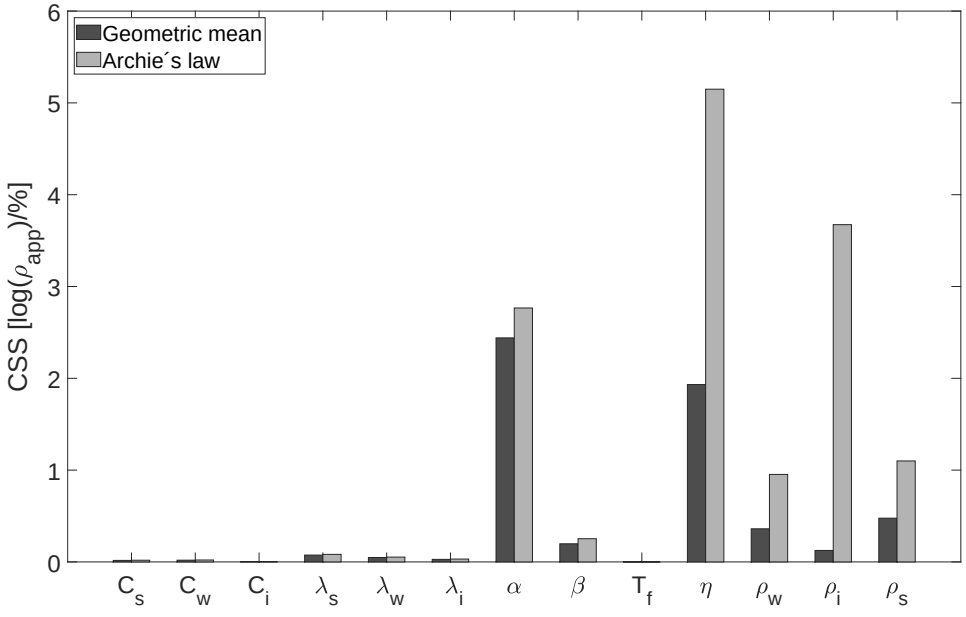

Figure 7. Composite scaled sensitivities (CSS) of the 13 parameters of the heat and the resistivity modules of the fully coupled inversion scheme. The sensitivity is expressed as change in logarithm of forward-calculated apparent resistivity following 10% change in the evaluated parameter.

Both petro-physical relationships showed relatively little sensitivity to changes in the heat model-only parameters C and λ. Porosity (η) was among the most influential parameters in the coupled scheme, as it was previously in the heat model alone. This makes sense, as the total volume (in addition to inter-connectedness) of pores available for storage and movement of soil moisture determine resistance to current flow. In terms of the resistivity parameters (ρ_w for Archie's law and the geometric mean, ρ_i and ρ_s for the geometric mean only) and the parameters of soil freezing curve α and β, the Archie's formulation was more sensitive and therefore offered better chances at model calibration. We therefore proceeded with using the Archie's law as the petro-physical relationships in the resistivity module. This was in spite of the two extra parameters to calibrate in the

https://doi.org/10.5194/tc-2023-51
Preprint. Discussion started: 6 April 2023


The Cryosphere Discussions
Open Access
EGU

Archie's law (m and n). Following these considerations as well as the experience from heat model calibration, we identified our target parameters for optimization as the following: λ_s, α, β, η, ρ_w, m and n.

Parameter optimization in the coupled inversion scheme is based on the same approach as in the heat modeling alone: the iterative non-linear least-squares formulation using the trust-region reflective algorithm. The cost function is the RMSE between logarithms of field-measured and forward-calculated *apparent resistivities*. We use log-transformed resistivities, as this way the optimization problem becomes more linear and a more equally weighted fitting of the resistivity data is achieved. The cost function is minimized by adjusting thermal parameters of the heat model from which the forward resistivities are calculated, as well as the parameters of the resistivity model.

7.2 Validation on synthetic data

We performed several optimization runs on synthetic data without noise, to get a feel for the sensitivity of the optimization algorithm, correct optimization settings and identify the combination of parameters that can be estimated at once. In the procedure common with the heat model testing (Sect. 6.3), a set of arbitrary though realistic parameter values (termed *true parameters*) was used to produce a *reference temperature field*, which in turn produced the corresponding *synthetic effective resistivity model* of the ground. From this synthetic resistivity model, *reference apparent resistivity* response was calculated. The true parameter value(s) were then perturbed by a random error coefficient ranging from $\pm 20 - 90\%$. We then aimed to recover the true parameter values by updating the perturbed heat and resistivity parameters iteratively, and comparing the forward-calculated synthetic apparent resistivity to the reference apparent resistivity. The optimization algorithm and the convergence criteria were the same as described in the analogous section on the heat model testing (Sect. 6.3).

Porosity η as the most sensitive parameter of the coupled model was recovered accurately within 3 iterations and with narrow 95% confidence intervals. Thermal conductivity of soil grains λ_s is an essential parameter for heat model predictions, even though the coupled scheme appeared to be very little sensitive to it. Nevertheless, in a single-parameter optimization on synthetic data without noise, the true parameter value was recovered accurately within 4 iterations. Joint calibration of all of the 7 fitted parameters at once – α, β, η, λ_s, ρ_w, m, n – converged within 4 –5 iterations, depending on the starting values, while producing very good fit between simulated and reference apparent resistivities (final RMSE after optimization in the range of 10^{-3} – 10^{-2}). However, in spite of the good model fit, the true parameter values were not accurately recovered and their optimized values depended on their starting values. In spite of the non-unique results of the inversion, all the optimized parameters lied in physically plausible range.

To improve the accuracy of recovery of the true parameters in the synthetic scenario, we experimented with fixing some of the less sensitive parameters of the coupled scheme. The optimization with 6 fitted parameters (α, β, η, ρ_w, m, n) and C_s and λ_s fixed, produced slightly lower final RMSE in comparison to the optimization with 7 and 5 fitted parameters; however, it did not improve recovery of the true parameter values. We noted that the coupled inversion scheme may not arrive at a unique estimation of the accurate parameter values; nevertheless, our synthetic tests confirmed that the optimization algorithm repeatedly converged to a set of physically plausible parameters while producing very good fit with the reference dataset.

https://doi.org/10.5194/tc-2023-51
Preprint. Discussion started: 6 April 2023

In the following section, we applied the fully coupled inversion approach to recovery of thermal and resistivity parameters of the real ground, and we compared the results to the traditional method of calibration on borehole temperatures only.

7.3 Fully coupled inversion with field data

Following the experience from synthetic testing (Sect. 7.2), we chose to optimize 6 fitted parameters at once: α, β, η, ρ_w, m, and n. We fixed the thermal conductivity λ_s to value 1.70 W/m/K and the heat capacity C_s to 3e^6 J/m^3/K (values from heat model calibration RMSE1, section 6.4).

The results of the 6-parameter optimization on field resistivity data are shown on Fig. 8. Fig. 8a shows the best fit of apparent resistivities after calibration on freezing season 2014/2015. Although the fit between simulated and field apparent resistivities is not ideal, the optimized parameterization produces temperature field that fits the field temperatures in freezing season 2014/2015 within $\pm 0.66°$(Fig. 8b).

To assess the predictive value of the model, we used the optimized parameterization estimates (values as listed in Fig. 8a and 8b) to forward-calculate the apparent resistivity distribution in the freezing seasons 2012/2013 (Fig. 8c) and 2013/2014 respectively (Fig. 8e). The parameter values optimized on the freezing season 2014/2015 predicted the field temperature measurements from freezing season 2012/2013 with mean error $0.38\,°\mathrm{C}$ (Fig. 8d). The field temperature measurements from freezing season 2013/2014 (only two months are available for comparison) were predicted with mean error $0.30\,°\mathrm{C}$ (Fig. 8f).

In terms of the model fit, the performance of the coupled optimization approach is comparable to the traditional optimization on borehole temperatures 6.4). In terms of determination true parameters of the real ground, the coupled inversion approach does not improve the non-uniqueness of parameter optimization; the optimized parameter values depend on their initial parameter estimates. Nevertheless, all the optimization runs come up with physically plausible parameter values and the forward-calculated temperature fields fit the field datasets with mean error of around $0.6\,°\mathrm{C}$.

8 Discussion

Efforts using geophysical data to constrain other – especially hydrological – models are by now well documented. The coupling strategies vary, from constraining inversion and interpretation of the other models with inverted geophysical data (Doetsch et al., 2013), through structurally-coupled approaches (Gallardo and Meju, 2011; Lochbühler et al., 2013), to fully coupled inversion schemes using the geophysical data before inversion (Hinnell et al., 2010; Herckenrath et al., 2013b; Tran et al., 2017). The fully coupled approaches have been encouraged by some (Gallardo and Meju, 2011), as separate data inversions lead to inconsistent models for the same subsurface target. The fully coupled framework has been shown to improve accuracy and reduce uncertainty of prediction of hydrological parameters (Hinnell et al., 2010; Herckenrath et al., 2013a)

Whether a certain model fulfills its purpose (i.e. whether it is a *good model*) depends on an outcome of validation. While the validation is not necessarily a required part of model development (Mankin et al., 1975), it helps in determining the domain over which the model is applicable and increases model's credibility. According to Rykiel (1996), validation means that a model is

https://doi.org/10.5194/tc-2023-51
Preprint. Discussion started: 6 April 2023

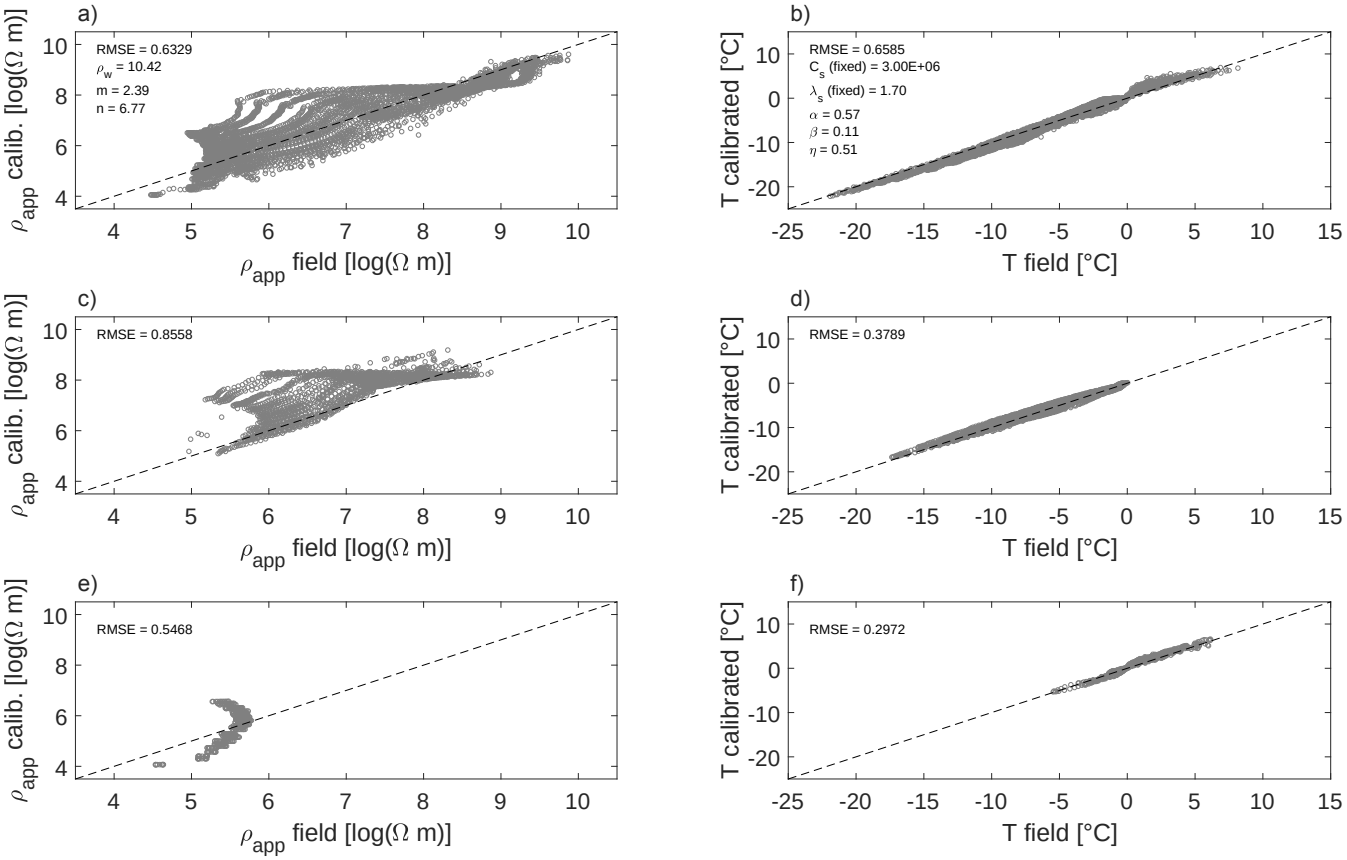

Figure 8. Results of the fully coupled inversion: a) and b) show results of calibration, c) through f) show results of validation. a) Fit of the simulated apparent resistivities (ρ_{app}) to field ρ_{app} measured during freezing season 2014 – 2015; b) fit of the heat model after optimization, freezing season 2014 – 2015. c) and d) Validation of the optimized coupled model on freezing season 2012 – 2013. e) and f) Validation of the optimized coupled model on freezing season 2013 – 2014 (e and f). Values of the fixed and optimized thermal and resistivity model parameters are listed in annotations.

https://doi.org/10.5194/tc-2023-51
Preprint. Discussion started: 6 April 2023

acceptable for its intended use because it meets specified performance requirements. Thus before validation is undertaken, the following criteria must be clarified: i) the purpose of the model, ii) the performance criteria, and iii) the model context.

In permafrost studies, the purpose of a model typically is forecasting long-term permafrost response to change in environmental conditions, such as climate forcing. The task is to come up with a model that reproduces a training dataset within certain error bounds accepted by the modeler. The underlying assumption is that such model has succeeded in capturing the main structural and conceptual features of the modeled object; if the climate forcing is the only changing variable, the model should be able to predict system's response under changing boundary conditions with known uncertainty.

However, purely the fact that a model can match a set of calibration data does not guarantee its predictive value. In fact, it can well be expected that a dataset forward-calculated with the true set of parameter values would *not* produce the lowest RMSE when compared to field data containing noise. Due to the relatively large number of fitted parameters, uncertainty and noise in calibration data and assumptions and simplifications in conceptual model, it is *always* possible to come up with a model that fits a given set of training data within reasonable error bounds. Indeed, we documented non-unique parameter estimation and wide spread of optimized parameter values depending on their initial guess, all producing equally good model fit (Fig. 4). Nicolsky et al. (2007) stressed the importance of good initial parameterization estimates when using gradient-search methods. Using their approach to determining optimal initial parameter estimates that are likely in the basin of attraction of global minimum may help narrowing down plausible parameter combinations. Depending on the context and intended application though, the predictive value of the coupled model is an encouraging result.

Conceptual simplifications of the heat model could present one of the immediate ways for improving performance of the coupled framework. We tested a heterogeneous model setup, accounting for different thermal properties due to varying ice content in the active layer vs. top of permafrost. The use of the more complex model was not justified by improved performance, neither in terms of model fit nor in uniqueness of parameter estimation.

The use of Archie's law is usually limited to sediments with low clay content, when virtually all conductivity in the bulk soil can be attributed to the pore liquid. This condition is not entirely met in our field situation, as high clay content may contribute to lowering the overall soil resistivity by surface conduction. We did test a modification of Archie's law accounting for surface conduction of clays (e.g. Glover et al. (2000)); however, the results did not justify proceeding with this version of petrophysical relationship. Adaptation of the resistivity mixing relationship remains a possibility for improvement of performance of the coupled inversion framework.

The approach described in this work constitutes one of a number of possible ways of adding a constraining information directly to the process of estimation of heat model parameters. The field geoelectrical data were shown to contain constraining information for calibration of the heat model. Even though we did not obtain an ideal resistivity model, the thermal calibration was useful. The fit and predictive performance of the resistivity-calibrated heat model was comparable to the fit of heat model calibrated on borehole temperature measurements.

https://doi.org/10.5194/tc-2023-51
Preprint. Discussion started: 6 April 2023

9 Conclusions

As the main conclusion of our study, we demonstrated the feasibility of calibrating the ground thermal model with field, time-lapse geoelectrical data collected from the ground surface. This is the first time that field data have been used to demonstrate that the concept of the fully coupled thermo-geophysical inversion can work in praxis. The fully coupled model achieved performance comparable to the traditional method of calibration on borehole temperatures.

In the process, we thoroughly evaluated a comparatively simple (1D, homogeneous, 3-phase) model for heat transfer in a ground undergoing cycles of freezing and thawing. The model relies on a number of conceptual assumptions to maintain parsimony. Nevertheless, it predicts temperature variation at our test site with satisfactory accuracy – within $0.55\,^{\circ}\mathrm{C}$. Simplicity of the model is a benefit in that the requirements on input data are relatively low – only surface temperature timeseries (measured, or downscaled from air temperature data), initial temperature distribution and bottom boundary condition are needed. On the other hand, it has to be expected that the final, optimized parameter estimates will compensate for conceptual simplifications of the model.

In the context of geotechnical and engineering applications (such as forecasting stability of infrastructure built on thawing permafrost), the true values of thermal parameters remain of interest, as they can be used further in geotechnical models. Further efforts in improving the structure and sensitivity of the model, constraining the optimization and including further independent validation will be required to validate the model in this context.

Although we advocate for use of easy-to-measure ground surface temperatures to drive the model, we do recognize that these typically suffer from rapid fluctuations influenced by short-wave radiation. Using near-surface temperatures to drive the model instead (at ca. 10 cm depth) could improve performance in the upper portion of the modeled domain.

Due to hysteretic nature of freeze-thaw processes, the heat model needs to be calibrated for freezing and thawing seasons separately. The relatively short timeseries of one freezing season (180 days) were sufficient to reach a plausible parameter estimation for the freezing season providing good fit to the validation dataset.

With the constantly improving understanding of electrical resistivity responses in the very specific permafrost settings, the resistivity coupling with thermal models opens up new possibilities for monitoring the current and forecasting the future thermal state of permafrost. The method has the demonstrated potential for offering a more resource-efficient alternative to calibration of ground thermal models on borehole temperature records.

Author contributions. ST conducted the data treatment, modeling and wrote the manuscript. TIN implemented the SOILFREEZE1D solver for heat conduction and contributed to the intellectual content of the manuscript. Both authors contributed to development of the coupled inversion scheme.

Competing interests. No competing interests are present.

https://doi.org/10.5194/tc-2023-51
Preprint. Discussion started: 6 April 2023

485 *Acknowledgements.* This study was part of project TARAJULIK, funded by the Greenland Research Council, grant agreement 80.30. The study was also supported by the NUNATARYUK project, which is funded under the European Union's Horizon 2020 Research and Innovation Programme, grant agreement 773421.

https://doi.org/10.5194/tc-2023-51
Preprint. Discussion started: 6 April 2023

References

Anderson, D. M. and Tice, A. R.: Predicting unfrozen water contents in frozen soils from surface area measurements, Highway research record, 1972.

Anderson, D. M., Tice, A. R., and McKim, H. L.: The unfrozen water and the apparent specific heat capacity of frozen soils, in: Proceedings of the second international conference on permafrost; North American contribution. Natl Acad Sci, Washington, DC, pp. 289–295, 1973.

Archie, G. E. et al.: The electrical resistivity log as an aid in determining some reservoir characteristics, Transactions of the AIME, 146, 54–62, 1942.

Bennike, O. and Björck, S.: Chronology of the last recession of the Greenland Ice Sheet, Journal of Quaternary Science, 17, 211–219, 2002.

Brown, J., Ferrians Jr, O., Heginbottom, J., and Melnikov, E.: revised February 2001. Circum-Arctic map of permafrost and ground-ice conditions. Boulder, CO: National Snow and Ice Data Center/World Data Center for Glaciology, Digital media, 1998.

Cappelen, J.: Weather observations from Greenland 1958-2019. Observation data with description., Tech. Rep. 20-08, Danish Meteorological Institute, https://www.dmi.dk/publikationer/, 2020.

Coleman, T. F. and Li, Y.: An interior trust region approach for nonlinear minimization subject to bounds, SIAM Journal on optimization, 6, 418–445, 1996.

Doetsch, J., Kowalsky, M. B., Doughty, C., Finsterle, S., Ajo-Franklin, J. B., Carrigan, C. R., Yang, X., Hovorka, S. D., and Daley, T. M.: Constraining CO 2 simulations by coupled modeling and inversion of electrical resistance and gas composition data, International Journal of Greenhouse Gas Control, 18, 510–522, 2013.

Doetsch, J., Ingeman-Nielsen, T., Christiansen, A. V., Fiandaca, G., Auken, E., and Elberling, B.: Direct current (DC) resistivity and induced polarization (IP) monitoring of active layer dynamics at high temporal resolution, Cold Regions Science and Technology, 119, 16–28, 2015.

Friedman, S. P.: Soil properties influencing apparent electrical conductivity: a review, Computers and electronics in agriculture, 46, 45–70, 2005.

Gallardo, L. A. and Meju, M. A.: Structure-coupled multiphysics imaging in geophysical sciences, Reviews of Geophysics, 49, 2011.

Geoteknisk Institut: Borehole log 78020 Jakobshavn, Archive material available at Asiaq Greenland Survey, Nuuk, Greenland, 1978.

Glover, P. W., Hole, M. J., and Pous, J.: A modified Archie's law for two conducting phases, Earth and Planetary Science Letters, 180, 369–383, 2000.

Guéguen, Y. and Palciauskas, V.: Introduction to the physics of rocks, Princeton University Press, 1994.

Harris, C., Arenson, L. U., Christiansen, H. H., Etzelmüller, B., Frauenfelder, R., Gruber, S., Haeberli, W., Hauck, C., Hoelzle, M., Humlum, O., et al.: Permafrost and climate in Europe: Monitoring and modelling thermal, geomorphological and geotechnical responses, Earth-Science Reviews, 92, 117–171, 2009.

Hauck, C.: Frozen ground monitoring using DC resistivity tomography, Geophysical research letters, 29, 2002.

Hauck, C., Bach, M., and Hilbich, C.: A 4-phase model to quantify subsurface ice and water content in permafrost regions based on geophysical datasets, in: Proceedings Ninth International Conference on Permafrost, June, pp. 675–680, 2008.

Herckenrath, D., Fiandaca, G., Auken, E., and Bauer-Gottwein, P.: Sequential and joint hydrogeophysical inversion using a field-scale groundwater model with ERT and TDEM data, Hydrology and Earth System Sciences, 17, 4043–4060, 2013a.

https://doi.org/10.5194/tc-2023-51
Preprint. Discussion started: 6 April 2023

Herckenrath, D., Odlum, N., Nenna, V., Knight, R., Auken, E., and Bauer-Gottwein, P.: Calibrating a Salt Water Intrusion Model with Time-Domain Electromagnetic Data, Groundwater, 51, 385–397, 2013b.

Hill, M. C.: Methods and guidelines for effective model calibration, US Geological Survey Denver, CO, USA, 1998.

Hinnell, A., Ferré, T., Vrugt, J., Huisman, J., Moysey, S., Rings, J., and Kowalsky, M.: Improved extraction of hydrologic information from geophysical data through coupled hydrogeophysical inversion, Water resources research, 46, 2010.

Hoekstra, P., Sellmann, P. V., and Delaney, A.: Ground and airborne resistivity surveys of permafrost near Fairbanks, Alaska, Geophysics, 40, 641–656, 1975.

Ingeman-Nielsen, T.: Geophysical techniques applied to permafrost investigations in Greenland, Ph.D. thesis, BYG. DTU, 2005.

Ingeman-Nielsen, T. and Baumgartner, F.: CR1Dmod: A matlab program to model 1D complex resistivity effects in electrical and electromagnetic surveys, Computers & Geosciences, 32, 1411–1419, 2006.

Jafarov, E. E., Harp, D. R., Coon, E. T., Dafflon, B., Tran, A. P., Atchley, A. L., Lin, Y., and Wilson, C. J.: Estimation of subsurface porosities and thermal conductivities of polygonal tundra by coupled inversion of electrical resistivity, temperature, and moisture content data, The Cryosphere, 14, 77–91, 2020.

Jessen, S., Holmslykke, H. D., Rasmussen, K., Richardt, N., and Holm, P. E.: Hydrology and pore water chemistry in a permafrost wetland, Ilulissat, Greenland, Water Resources Research, 50, 4760–4774, 2014.

Johansen, O.: Thermal conductivity of soils, Tech. rep., Cold Regions Research and Engineering Lab Hanover NH, 1977.

Krautblatter, M., Verleysdonk, S., Flores-Orozco, A., and Kemna, A.: Temperature-calibrated imaging of seasonal changes in permafrost rock walls by quantitative electrical resistivity tomography (Zugspitze, German/Austrian Alps), Journal of Geophysical Research: Earth Surface, 115, 2010.

Lochbühler, T., Doetsch, J., Brauchler, R., and Linde, N.: Structure-coupled joint inversion of geophysical and hydrological data, Geophysics, 78, ID1–ID14, 2013.

Lovell Jr, C.: Temperature effects on phase composition and strength of partially-frozen soil, Highway Research Board Bulletin, 1957.

Lunardini, V. J.: Heat transfer in cold climates, Van Nostrand Reinhold Company, 1981.

Mankin, J., O'Neill, R., Shugart, H., and Rust, B.: The importance of validation in ecosystem analysis, New directions in the analysis of ecological systems, part, 1, 309–317, 1975.

Nicolsky, D., Romanovsky, V., and Tipenko, G.: Using in-situ temperature measurements to estimate saturated soil thermal properties by solving a sequence of optimization problems, The Cryosphere, 1, 41–58, 2007.

Nicolsky, D., Romanovsky, V., and Panteleev, G.: Estimation of soil thermal properties using in-situ temperature measurements in the active layer and permafrost, Cold Regions Science and Technology, 55, 120–129, 2009.

Obu, J., Westermann, S., Bartsch, A., Berdnikov, N., Christiansen, H. H., Dashtseren, A., Delaloye, R., Elberling, B., Etzelmüller, B., Kholodov, A., et al.: Northern Hemisphere permafrost map based on TTOP modelling for 2000–2016 at 1 km2 scale, Earth-Science Reviews, 2019.

Oldenborger, G. A. and LeBlanc, A.-M.: Monitoring changes in unfrozen water content with electrical resistivity surveys in cold continuous permafrost, Geophysical Journal International, 215, 965–977, 2018.

Osterkamp, T.: Freezing and thawing of soils and permafrost containing unfrozen water or brine, Water Resources Research, 23, 2279–2285, 1987.

Overduin, P. P., Kane, D. L., and van Loon, W. K.: Measuring thermal conductivity in freezing and thawing soil using the soil temperature response to heating, Cold Regions Science and Technology, 45, 8–22, 2006.

https://doi.org/10.5194/tc-2023-51
Preprint. Discussion started: 6 April 2023

Pedersen, L. L.: The mechanical properties of a saline fine-grained permafrost soil, Bc. thesis, Technical University of Denmark, Denmark, 2013.

Pellet, C. and Hauck, C.: Monitoring soil moisture from middle to high elevation in Switzerland: set-up and first results from the SOMOMOUNT network, Hydrology and Earth System Sciences, 21, 3199–3220, 2017.

Pellet, C., Hilbich, C., Marmy, A., and Hauck, C.: Soil moisture data for the validation of permafrost models using direct and indirect measurement approaches at three alpine sites, Frontiers in Earth Science, 3, 91, 2016.

Power, M.: The predictive validation of ecological and environmental models, Ecological modelling, 68, 33–50, 1993.

Riseborough, D., Shiklomanov, N., Etzelmüller, B., Gruber, S., and Marchenko, S.: Recent advances in permafrost modelling, Permafrost and Periglacial Processes, 19, 137–156, 2008.

Romanovsky, V., Osterkamp, T., et al.: Effects of unfrozen water on heat and mass transport processes in the active layer and permafrost, Permafrost and Periglacial Processes, 11, 219–239, 2000.

Rykiel, E. J.: Testing ecological models: the meaning of validation, Ecological modelling, 90, 229–244, 1996.

Tomaskovicova, S.: Coupled thermo-geophysical inversion for permafrost monitoring, 2018.

Tomaškovičová, S. and Ingeman-Nielsen, T.: Quantification of freeze-thaw hysteresis of unfrozen water content and electrical resistivity from time lapse measurements in the active layer and permafrost, Permafrost and Periglacial Processes, in review.

Tomaškovičová, S., Paamand, E., Ingeman-Nielsen, T., and Bauer-Gottwein, P.: Coupled thermo-geophysical inversion for permafrost monitoring, in: Xth International Conference on Permafrost, Salekhard, Russian Federation, pp. 587–588, 2012.

Tran, A. P., Dafflon, B., and Hubbard, S. S.: Coupled land surface–subsurface hydrogeophysical inverse modeling to estimate soil organic carbon content and explore associated hydrological and thermal dynamics in the Arctic tundra, The Cryosphere, 11, 2089–2109, 2017.

Zhang, Y., Carey, S. K., and Quinton, W. L.: Evaluation of the algorithms and parameterizations for ground thawing and freezing simulation in permafrost regions, Journal of Geophysical Research: Atmospheres, 113, 2008.